Nonequilibrium hadronization and constituent quark number scaling

Sven Zschocke,[1] Szabolcs Horvát,[2,3] Igor N. Mishustin,[4,5] and László P. Csernai[2,4,6]

[1]*TU Dresden, Institut für Planetare Geodäsie, Lohrmann-Observatorium, D-01062 Dresden, Germany*
[2]*Department of Physics and Technology, University of Bergen, Allegaten 55, N-5007 Bergen, Norway*
[3]*Faculty of Physics, Babes-Bolyai University, Kogalniceanu str 1, 400084 Cluj-Napoca, Romania*
[4]*Frankfurt Institute for Advanced Studies (FIAS), D-60438 Frankfurt am Main, Germany*
[5]*Russian Research Center, Kurchatov Institute, 123182 Moscow, Russia*
[6]*MTA–KFKI Research Institute for Particle Physics and Nuclear Physics, H-1525 Budapest, Hungary*

(Received 18 November 2010; revised manuscript received 17 January 2011; published 8 April 2011)

The constituent quark number scaling of elliptic flow is studied in a nonequilibrium hadronization and freeze-out model with rapid dynamical transition from ideal, deconfined, and chirally symmetric quark-gluon plasma, to final noninteracting hadrons. In this transition a bag model of constituent quarks is considered, where the quarks gain constituent quark mass while the background bag field breaks up and vanishes. The constituent quarks then recombine into simplified hadron states, while chemical, thermal, and flow equilibrium break down one after the other. In this scenario the resulting temperatures and flow velocities of baryons and mesons are different. Using a simplified few source model of the elliptic flow, we are able to reproduce the constituent quark number scaling, with assumptions on the details of the nonequilibrium processes.

DOI: 10.1103/PhysRevC.83.044903 PACS number(s): 25.75.Ld, 12.38.Mh, 24.10.Nz, 47.75.+f

I. INTRODUCTION

It was observed that the momentum distribution of particles created in heavy-ion collisions is not azimuthally symmetric in the plane perpendicular to the beam direction. This dominant asymmetry, the elliptic flow, is the result of several factors, the main one being the anisotropy of the initial configuration after the collision due to the nonzero impact parameter. The elliptic flow is typically characterized using the second coefficient of the Fourier expansion of the momentum distribution, v_2. It was found in experiments [1] that the v_2 parameter as a function of the transverse momentum, p_t, scales with the number of constituent quarks, n_{cq}, in a hadron; that is, if the $v_2(p_t)$ curves are rescaled according to the constituent quark number of the considered hadron species, and v_2/n_{cq} is plotted as a function of p_t/n_{cq} for each type of hadron with mass m_h, the curves will coincide. Later results showed that the scaling is more precise if v_2 is plotted as a function of the transverse kinetic energy, $E_t = \sqrt{m_h^2 + {p_t}^2} - m_h$, instead of the transverse momentum p_t.

This experimentally found scaling law is remarkably simple, and indicates that the elliptic flow develops before the quarks recombine into hadrons. Therefore, understanding the factors influencing the measurable v_2 can provide information about the state of the quark-gluon plasma (QGP).

The fluid dynamical (FD) model describes the dynamical development of the quark-gluon plasma from the (already thermalized) initial state until the breakdown of the equilibrium, where first the chemical equilibrium among quarks and antiquarks ceases. Initially the plasma has only two flavors, u and d, and thus the FD model assumes two flavors. However, the flavor equilibration in the plasma is a rapid process with a time scale of the order of 1 fm/c, so by the end of the FD development a flavor equilibrium among three flavors, u, d, and s, is reached. Our usual FD evolution does not take into account this chemical change of flavors with an additional rate equation; instead this process is taken into account at the final stage of the FD development, when the subsequent EoS is already assumed to have three equilibrated flavors. Energy and momentum conservation and the requirement of nondecreasing entropy is enforced in the transition, from the ideal quark-gluon plasma state to the state where quark and antiquark numbers are frozen out. As a consequence, the mass change of the quarks starts in the initial QGP with two flavors, and we use this approximation to estimate the final boundary where the initial FD stage of the evolution ends, with light quark masses.

We consider a model of hadronization and investigate the constituent quark number scaling (QNS) of the v_2 parameter. In this model, a gas of quarks and antiquarks expands in a background field represented by the bag constant B, which depends on density and temperature of the expanding fireball. Initially, this B field includes the energy of the deconfined perturbative vacuum and of the gluon fields. As the system expands the deconfinement starts and the average B decreases. Furthermore, as the chiral symmetry breaking starts, the quarks gain mass. The quark mass is calculated as a function of the temperature and density of the matter. The quark gas expands rapidly while the quark mass increases. This process can be considered as a simple representation of the breaking chiral symmetry and deconfinement in a dynamical transition crossing the Quarkyonic phase [2].

The point during the expansion when the quarks recombine into hadrons is determined from the condition that the average hadron energy is equivalent to (1.0–1.1) GeV, as found from the systematics of experimental data [3]. At recombination, the thermal and flow equilibrium between particles is broken.

Finally, the v_2 parameter is determined using simple two- and three-source models of the elliptic flow and the particle distributions obtained from the hadronization model.

The paper is organized as follows: In Sec. II the density and temperature dependence of constituent quark mass is considered. The energy, entropy, momentum, and chemical potential of each individual source and of the total source is given in

Sec. III. In Sec. IV we describe the used nonequilibrium model of rapid hadronization. Details of calculation of elliptic flow parameter v_2 are presented in Sec. V. A summary is given in Sec. VI.

II. CONSTITUENT QUARK MASS

To present our arguments we consider the Nambu-Jona-Lasinio model (NJL) which is motivated by quantum chromodynamics (QCD) and is basically a quark-quark interaction theory of quark fields q_f with flavor f; a comprehensive overview about NJL was presented in Ref. [4]. The extended NJL model contains three types of quark-quark interaction and is given by the Lagrangian [7]

$$\begin{aligned}\mathcal{L}_{\rm NJL} = &\sum_{f=u,d,s} \overline{q}_f(i\,\gamma^\mu\partial_\mu - m_f)q_f \\ &+ \frac{G_S}{2}\sum_{f=u,d,s}\sum_{a=0}^{8}[(\overline{q}_f\lambda^a q_f)^2 + (\overline{q}_f\, i\,\gamma_5\,\lambda^a q_f)^2] \\ &- \frac{G_V}{2}\sum_{f=u,d,s}\sum_{a=0}^{8}[(\overline{q}_f\,\gamma_\mu\,\lambda^a q_f)^2 + (\overline{q}_f\,\gamma_5\,\gamma_\mu\,\lambda^a q_f)^2] \\ &+ \frac{G_D}{2}[\det(\overline{q}_f(1+\gamma_5)q_f) + \det(\overline{q}_f(1-\gamma_5)q_f)],\end{aligned} \tag{1}$$

where $\overline{q}_f = q_f^\dagger\,\gamma_0$, γ^μ are the Dirac matrices, m_f is the current quark mass of flavor f, G_S is the coupling constant of the scalar-current interaction, G_V is the coupling constant of the vector-current interaction terms, and G_D is the coupling constant of the determinantal flavor-mixing term (determinant in flavor space). The Gell-Mann matrices are λ^a where $a = 0, 1, 2, \ldots, 8$ with $\lambda^0 = \sqrt{2/3}\,I$, where I is the unit matrix. This Lagrangian is used to derive the relation between constituent quark masses and chiral condensates, both for vacuum and for finite densities and temperatures.

A. Constituent quark mass in vacuum

First, we consider the constituent quark mass in vacuum. For three flavors, $SU_f(3)$, the constituent quark masses in vacuum $M_f^0 = M_f\,(n_B = 0, T = 0)$ where $f = u, d, s$, are related to the chiral condensates in vacuum as follows [5–7]:

$$M_u^0 = m_u - 2\,G_S\,\langle\overline{u}u\rangle_0 - G_D\,\langle\overline{d}d\rangle_0\,\langle\overline{s}s\rangle_0, \tag{2}$$

$$M_d^0 = m_d - 2\,G_S\,\langle\overline{d}d\rangle_0 - G_D\,\langle\overline{u}u\rangle_0\,\langle\overline{s}s\rangle_0, \tag{3}$$

$$M_s^0 = m_s - 2\,G_S\,\langle\overline{s}s\rangle_0 - G_D\,\langle\overline{u}u\rangle_0\,\langle\overline{d}d\rangle_0. \tag{4}$$

Here, $\overline{u} = u^\dagger\,\gamma_0$ and so on, $m_u = 5$ MeV, $m_d = 9$ MeV, and $m_s = 130$ MeV are the current quark masses of the u-quark, d-quark, and s-quark, respectively. Typical values of the chiral condensates in vacuum are given by, for example, [8,10] and references therein:

$$\langle\overline{q}q\rangle_0 = \langle\overline{u}u\rangle_0 = \langle\overline{d}d\rangle_0 = -(0.225\ \text{GeV})^3, \tag{5}$$

$$\langle\overline{s}s\rangle_0 = 0.7\,\langle\overline{u}u\rangle_0. \tag{6}$$

Typical values for the coupling constants are $G_S = (15$–$20)\ \text{GeV}^{-2}$, $G_V \simeq 0.5\,G_S$, and $G_D = -\,(160$–$240)\ \text{GeV}^{-5}$ [4,6,7]. We note that in relations (2)–(4) the magnitude of terms proportional to G_D are small compared to the terms proportional to G_S.

B. Constituent quark mass in a hot and dense medium

Let us now consider the case of quarks in a hot and dense medium, at early times of FD evolution. At this stage we assume to have two flavors. Then, the relations (2)–(4) for two flavors $SU_f(2)$ are reduced to

$$M_f = m_f - 2\,G_S\,\langle\overline{q}q\rangle_{n_B,T}. \tag{7}$$

The suffix n_B, T at chiral condensate denotes the Gibbs average over eigenstates of the effective theory, see Refs. [9,11–13] and references therein. Note that for isospin-symmetric matter there is no difference in the density and temperature dependence of u-quark and d-quark condensate, that means $\langle\overline{q}q\rangle_{n_B,T} \equiv \langle\overline{u}u\rangle_{n_B,T} = \langle\overline{d}d\rangle_{n_B,T}$. In the limit of high densities and temperatures the constituent quark mass, M_f, approaches the current quark mass, m_f. The well-known model-independent linear density dependence of the chiral condensate has widely been applied in many investigations (e.g., [7,8,12,15]). The temperature dependence of the chiral condensate was determined up to order $\mathcal{O}(T^8)$ in Ref. [16]. To determine the density *and* temperature dependence of the chiral condensate we follow the arguments of Refs. [7,12,14], where the first leading terms in the low-density low-temperature expansion have been obtained:

$$\begin{aligned}\langle\overline{q}q\rangle_{n_B,T} = \langle\overline{q}q\rangle_0\Bigg(1 - \frac{3\,\sigma_q}{f_\pi^2\,m_\pi^2}\,n_B - \frac{T^2}{8\,f_\pi^2} - \frac{T^4}{384\,f_\pi^4} \\ - \frac{T^6}{288\,f_\pi^6}\,\ln\frac{\Lambda_q}{T}\Bigg).\end{aligned} \tag{8}$$

The temperature and density dependence of chiral condensate was plotted in Ref. [14]. The baryonic density in terms of quark degrees of freedom is given by

$$n_B = \frac{1}{3}\sum_{f=u,d}(n_f - \overline{n}_f), \tag{9}$$

where n_f ($\overline{n}_f$) is the quark (antiquark) density. The baryonic density in a given volume V is related to the conserved baryon number N_B by $n_B = \frac{N_B}{V}$; note the relation $\hbar\,c = 197.3\,\text{MeV fm}$. For the logarithmic scale we take $\Lambda_q \simeq 300$ MeV; for details, see Ref. [16]. The pion mass in vacuum is $m_\pi = 138$ MeV and the pion decay constant in vacuum is $f_\pi = 93$ MeV. The numerical value of the quark-sigma term is $\sigma_q = 15$ MeV (see, e.g., Ref. [7]), which is three times smaller than the nucleon-sigma term $\sigma_N = 45$ MeV.

By combining Eq. (7) with Eq. (8), we obtain the expression for the in-medium mass of constituent quarks:

$$\begin{aligned}M_f = m_f - 2\,G_s\langle\overline{q}q\rangle_0\Bigg(1 - \frac{3\,\sigma_q}{f_\pi^2\,m_\pi^2}\,n_B - \frac{T^2}{8\,f_\pi^2} \\ - \frac{T^4}{384\,f_\pi^4} - \frac{T^6}{288\,f_\pi^6}\,\ln\frac{\Lambda_q}{T}\Bigg).\end{aligned} \tag{10}$$

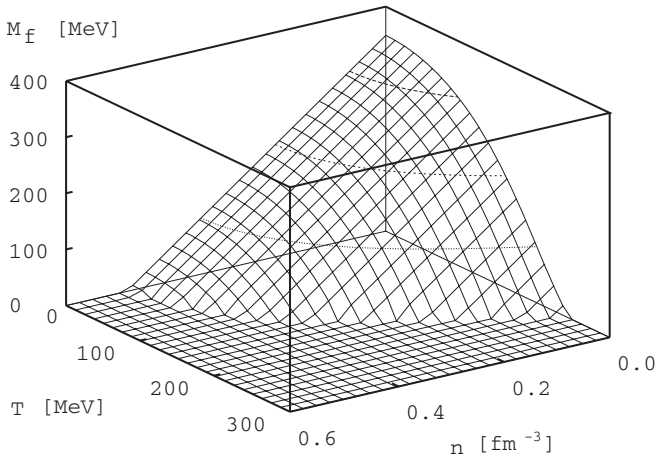

FIG. 1. Temperature and density dependence of the constituent quark mass M_f according to Eq. (10).

The temperature and density dependence of the constituent quark mass is plotted in Fig. 1. According to Eq. (10), for sufficiently high temperatures and densities the constituent quark mass will coincide with the current-quark-mass m_f. Of course, the applicability of Eq. (10) is restricted to low densities and temperatures. In any case, the most upper limit for density and temperature is given by the condition that constituent quark mass has to be positive.

III. EXPANDING QUARK-ANTIQUARK BAG

The bag consists of quarks, antiquarks, and the gluon fields. Nonperturbative effects in the QCD vacuum and the energy density of gluon fields are described by the bag constant, B. In our model, we subdivide the bag into N individual cells, each of which moves with an individual flow velocity $\boldsymbol{v}_i$.

A. Total energy of the bag

The total energy of the bag in the center-of-mass frame of the colliding nuclei is given by the volume integral of the "00" component of the energy momentum tensor of each cell i, $T_i^{\mu\nu} = (e^i + P^i)u_i^\mu u_i^\nu - P^i\, g^{\mu\nu}$. Considering that our EoS is given as a sum of the energy and pressure of the ideal quark and antiquark gas plus the uniform bag energy density B, that means $e^i = e_q^i + \overline{e}_q^i + B$ and $P^i = P_q^i + \overline{P}_q^i - B$, the total energy of all cells of the bag in the center-of-mass frame of the colliding nuclei is given by

$$E_{\text{total}} = \sum_{i=1}^{N} V^i\,(\gamma^i)^2(e^i + P^i) - \sum_{i=1}^{N} V^i\, P^i, \qquad (11)$$

where the sum runs over the number of all cells of the bag. Here, we assume a uniform bag-field energy density B over the whole volume, V; B depends on density and temperature of the bag, thus on the time of the evolution of the fireball. We have used the notation e^i for the invariant scalar, rest-frame energy density, and P^i for the scalar pressure, V^i is the volume of cell i in the center-of-mass frame, and $\gamma_i = 1/\sqrt{1-\mathbf{v}_i^2}$ where $\mathbf{v}_i$ is the 3-velocity of cell i. To determine the rest-frame energy or proper energy of the cells, we assume a Boltzmann-Jüttner distribution [17] for the particles inside each individual cell:

$$f_{\text{J}}^i = \frac{1}{(2\,\pi\,\hbar)^3}\,\exp\left(\frac{\mu^i - u_\mu^i\; p^\mu}{T_i}\right), \qquad (12)$$

and $\int d^3x \int d^3p\; f_J^i(\boldsymbol{x}, \boldsymbol{p}) = N_i$ is the normalization of the Jüttner distribution, where N_i is the number of particles of a given type inside cell i under consideration. The proper energy density is a Lorentz invariant quantity by definition and, therefore, can be evaluated in any frame (e.g., in the local rest frame). Accordingly, we obtain the following expression for the energy density of quarks and antiquarks for each cell of the bag:

$$e^i = e_q^i + \overline{e}_q^i + B, \qquad (13)$$

$$e_q^i = \frac{1}{8\,\pi^2}\sum_{f=u,d} M_f^3\; T_i\,\exp\left(\frac{\mu_q^i}{T_i}\right) \times\left[K_1\left(\frac{M_f}{T_i}\right) + 3K_3\left(\frac{M_f}{T_i}\right)\right], \qquad (14)$$

$$\overline{e}_q^i = \frac{1}{8\,\pi^2}\sum_{f=u,d} M_f^3\; T_i\,\exp\left(\frac{\overline{\mu}_q^i}{T_i}\right) \times\left[K_1\left(\frac{M_f}{T_i}\right) + 3K_3\left(\frac{M_f}{T_i}\right)\right]. \qquad (15)$$

Here, K_n are the Bessel functions of second kind [26]. The density and temperature-dependent constituent quark mass M_f is given in (10), and n_B^i and T_i are the baryonic density and temperature, respectively, of the cell i. The initial value of the bag constant is abbreviated by B_0, and we use the numerical value $B_0 = (198\ \text{MeV})^4 = 0.2\ \text{GeV fm}^{-3}$; see also considerations in Ref. [18].

B. Total entropy of the bag

The total entropy in the center-of-mass Lorentz frame (CM) is given by

$$S_{\text{total}} = \sum_{i=1}^{N} V^i\;\gamma^i\;s^i, \qquad (16)$$

where the sum runs over all cells of the bag. The invariant scalar entropy density, s^i, can be evaluated in any frame. The total entropy density consists of entropy density of the quarks and antiquarks, and for the assumed Jüttner distribution is given by

$$s^i = s_q^i + \overline{s}_q^i, \qquad (17)$$

$$s_q^i = \frac{1}{2\pi^2}\sum_{f=u,d} M_f^2\,\exp\left(\frac{\mu_q^i}{T_i}\right) \times\left[M_f\,K_1\left(\frac{M_f}{T_i}\right) + T_i\left(4 - \frac{\mu_q^i}{T_i}\right)K_2\left(\frac{M_f}{T_i}\right)\right], \qquad (18)$$

$$\overline{s}_q^i = \frac{1}{2\pi^2} \sum_{f=u,d} M_f^2 \exp\left(\frac{\overline{\mu}_q^i}{T_i}\right) \times \left[M_f\, K_1\left(\frac{M_f}{T_i}\right) + T_i\left(4 - \frac{\overline{\mu}_q^i}{T_i}\right) K_2\left(\frac{M_f}{T_i}\right)\right]. \quad (19)$$

In what follows, we will take the adiabatic limit, which implies the total entropy to be a constant. We note that there is no bag constant in the expression for the total entropy because the bag field is uniform (i.e., the entropy of the bag field vanishes).

C. Total momentum of the bag

The total momentum of the bag in the center-of-mass Lorentz frame is given by

$$0 = \boldsymbol{p}_{\text{total}} = \sum_{i=1}^{N} V^i\, (\gamma^i)^2\, (e^i + P^i)\boldsymbol{v}_i, \quad (20)$$

where the sum runs over all cells of the bag. The scalar pressure of each individual cell of the bag is given by

$$P^i = P_q^i + \overline{P}_q^i - B, \quad (21)$$

$$P_q^i = \frac{1}{2\pi^2} \sum_{f=u,d} M_f^2\, T_i^2 \exp\left(\frac{\mu_q^i}{T_i}\right) K_2\left(\frac{M_f}{T_i}\right), \quad (22)$$

$$\overline{P}_q^i = \frac{1}{2\pi^2} \sum_{f=u,d} M_f^2\, T_i^2 \exp\left(\frac{\overline{\mu}_q^i}{T_i}\right) K_2\left(\frac{M_f}{T_i}\right). \quad (23)$$

We note that there is no bag constant in the expression for the total momentum (20) because it cancels out in the sum $e^i + P^i$ according to Eqs. (13) and (21).

D. Chemical potential of quarks and antiquarks

Assuming a Jüttner distribution, the density $n_f^i = \frac{N_f^i}{V_i}$ of quarks having flavor f and the density of antiquarks $\overline{n}_f^i = \frac{\overline{N}_f^i}{V_i}$ having flavor f in a given cell i is determined by the following equations:

$$n_f^i = \frac{1}{2\pi^2} M_f^2\, T_i \exp\left(\frac{\mu_q^i}{T_i}\right) K_2\left(\frac{M_f}{T_i}\right), \quad (24)$$

$$\overline{n}_f^i = \frac{1}{2\pi^2} M_f^2\, T_i \exp\left(\frac{\overline{\mu}_q^i}{T_i}\right) K_2\left(\frac{M_f}{T_i}\right). \quad (25)$$

In mechanical (pressure), thermal, and chemical equilibrium, the number of quarks depends only on baryonic chemical potential μ_B and temperature T. Especially, if the quarks and antiquarks are in chemical equilibrium with each other, then $\mu_q = \mu_B/3$ and $\overline{\mu}_q = -\mu_B/3$. To determine the baryonic chemical potential μ_B we have to use the total baryonic number density n_B given in Eq. (9). Then, according to the expressions (24) and (25), we obtain a definition of the chemical potential μ_B^i of cell i as

$$n_B^i = \frac{1}{3\pi^2} T_i \sinh\left(\frac{\mu_B^i}{3\,T_i}\right) \sum_{f=u,d} M_f^2\, K_2\left(\frac{M_f}{T_i}\right), \quad (26)$$

where we have used $\sinh x = \frac{1}{2}(e^x - e^{-x})$. We assume that these thermodynamic relations hold in the ideal QGP until the final stage of the expansion starts. Then the net baryon number in each cell N_B^i and the number of quarks and antiquarks, $N_q^i = (n_u^i + n_d^i)V_i$ and $\overline{N}_q^i = (\overline{n}_u^i + \overline{n}_d^i)V_i$, respectively, are given. While V_i and thus n_f^i and $\overline{n}_f^i$ are changing during the expansion, the numbers of quarks and antiquarks, N_q^i and $\overline{N}_q^i$, are fixed at this point in each cell and do not change afterwards. This is the chemical freeze-out in the model.

The volumes, baryonic, and quark densities and temperatures of each individual cell change during the expansion. The chemical equilibrium between the baryon density and quark- and antiquark densities breaks down at this point. Consequently, the chemical potentials for the single quarks are related to the single quark (and antiquark) densities only and are not connected to the net baryon density. Although we need the chemical potentials for the calculation of the energy density, pressure, and entropy, these must be calculated from the given quark and antiquark densities in each cell, by using Eqs. (24) and (25), which determine μ_q^i and $\overline{\mu}_q^i$. The net baryon number n_B is conserved and is determined by Eq. (9) using Eqs. (24) and (25). Only in the case of chemical equilibrium Eq. (26) is used to determine the chemical potential μ_B; that is, the N_B/N_q and $N_B/\overline{N}_q$ ratio freezes out first at the initialization of our model calculation for the final expansion stage, where quarks start to gain mass, the background field B starts to disappear, but the constituent quark numbers do not change. The flow does not evolve, the cells expand while coasting with negligible pressure. Still considerable changes happen regarding the masses and temperatures of the system.

IV. NONEQUILIBRIUM EXPANSION STAGE

A. Rapid hadronization hypothesis

A first-order phase transition in chemical and thermal equilibrium with homogeneous nucleation would take a long time [19], longer than two-particle correlation measurements indicate. If the homogeneous nucleation cannot support the required rapid transition then the transition becomes delayed and freeze-out and hadronization will happen rapidly and simultaneously from a supercooled QGP. Thus, a rapid process must be out of equilibrium, at least of chemical equilibrium [20]. Possible detailed mechanisms of this out-of-equilibrium transition are addressed recently in several works [21,22]. In the framework of the present model this transition is represented by the mass gain and coalescence of constituent quarks, and the simultaneous disappearance of the bag field. These two processes are treated phenomenologically, while we enforce conservation laws and our model constraints.

Such a rapid, out-of-equilibrium process must result in additional entropy production [20] from the latent heat of the transition (just like at sudden condensation of supercooled vapor). We start with our model at the line where we have

quarks with current quark masses, and the process ends when we reach the empirical hadron freeze-out line, where quarks have constituent quark mass.

It was found by Cleymans *et al.* [3] that, in a wide range of beam energies, detected hadrons freeze-out and reach the detectors when the average energy of hadrons (estimated in a thermal, statistical equilibrium fireball model) is between $E_H/N_H = (1.0\text{–}1.1)$ GeV. Just at the freeze-out moment the particles do not interact any longer, so the ideal hadron gas mixture is a good approximation. Furthermore, if we plot the FO points on the temperature-chemical potential $[T, \mu_B]$ plane, the (1.0–1.1) GeV constant specific energy contours fall on a continuous line indicating that the final state is representing a statistical thermal equilibrium state of hadrons or a state which is close to it. At the FO state with vanishing interactions and dissipation the expansion of the fireball is adiabatic to a good approximation.

We can also approximate the final FO hadron state by assuming a Jüttner distribution to all hadrons; that means we use a relation between chemical potential μ_B and temperature T by means of average energy per hadron,

$$\frac{E_H}{N_H} = \frac{\sum_{h=1}^{N} e_h(m_h, T, \mu_h)}{\sum_{h=1}^{N} n_h(m_h, T, \mu_h)} = (1.0 - 1.1)\,\text{GeV}, \quad (27)$$

where hadronic energy density and hadronic particle density are given by

$$e_h = \frac{g_h}{4\pi^2} T \cosh\left(\frac{\mu_h}{T}\right) m_h^3 \left(K_1\left(\frac{m_h}{T}\right) + K_3\left(\frac{m_h}{T}\right)\right),$$
$$n_h = \frac{g_h}{\pi^2} T \sinh\left(\frac{\mu_h}{T}\right) m_h^2 K_2\left(\frac{m_h}{T}\right). \quad (28)$$

Here, m_h is the mass of the hadron, g_h is the degeneracy factor, and for baryons we have $\mu_h = \mu_B$ while for mesons $\mu_h = 0$. The Boltzmann-Jüttner gas approach is a good approximation to the full fluid dynamics and Boltzmann equation statistical result: In the medium $[T, \mu_B]$ range the FO contour lines are shown in Fig. 2(a); we have taken into account the lightest 100 hadrons, that is, $[h = \pi^0, \pi^\pm, K^0, K^\pm, ..., D(1950)]$.

In this transition the expansion of the quark gas continues until the average energy per hadron reaches about (1.0–1.1) GeV. In a statistical thermal equilibrium model this can be represented on the $[T, \mu_B]$ plane. In the present nonequilibrium model the thermal equilibrium is kept, but μ_B is not representative of the hadron multiplicity. However, we can approximate the Cleymans line by estimating the hadron multiplicity or density after coalescence of our constituent quarks into baryons and mesons. The freeze-out curve on the $[n_B, T]$ plane is plotted in Fig. 2(b).

The cold uniform nuclear matter has an equilibrium density of $n_B = (0.15\text{–}0.17)$ fm^{-3}, similar to the central density of large nuclei. At higher temperatures a considerable number of mesons are also present in statistical equilibrium, thus the *effective* baryon density for the same energy density decreases with increasing temperature. This enables us to construct an effective Cleymans freeze-out line on the $[T, n_B]$ plane for the purposes of our nonequilibrium model.

We have assumed that our rapid hadronization starts at the $[T, n_B]$ contour where our quarks have current quark mass of about 7 MeV. This contour is plotted in Fig. 3. The chemical equilibrium then ceases among quarks and antiquarks, and we neglect quark and antiquark annihilations in the final expansion stage. Thus, the total number of quarks and antiquarks, N_q and $\overline{N}_q$, remains constant (in contrast to the statistical thermal equilibrium model), while the baryon charge, $N_B = (N_q - \overline{N}_q)/3$, remains also constant as required by baryon conservation.

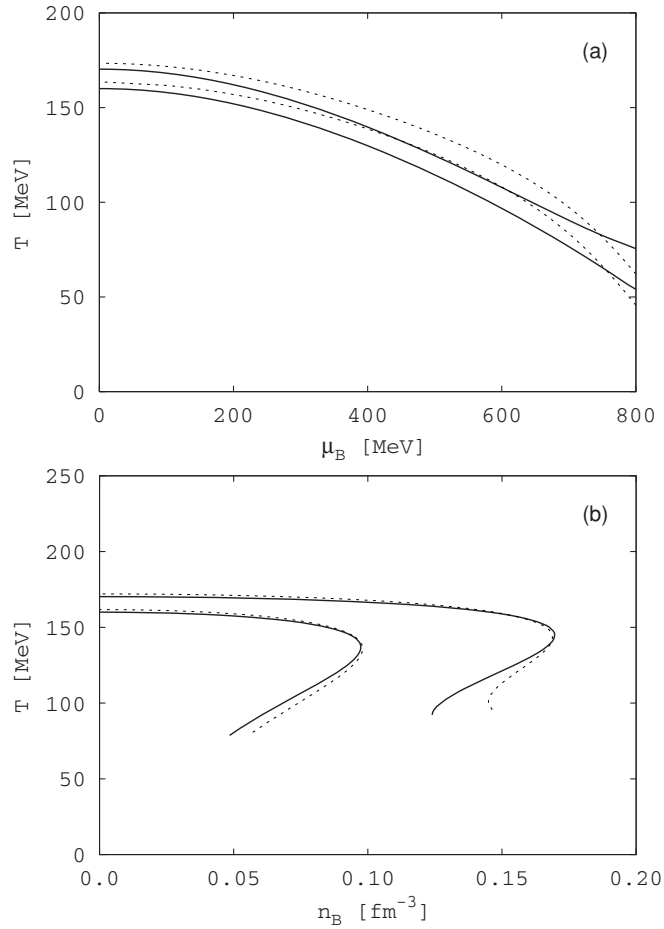

FIG. 2. (a) Shows the freeze-out curves on the $[\mu_B, T]$ plane, corresponding to mean energy $E_H/N_H = 1.0$ and 1.1 GeV per hadron. The solid lines were computed assuming that the hadrons have a Jüttner distribution; see Eq. (27) (upper solid curve for 1.1 GeV; lower solid curve for 1.0 GeV). The dotted lines are from the statistical thermal model [3] (upper dotted curve for 1.1 GeV; lower dotted curve for 1.0 GeV). (b) Shows the same curves transformed to the $[n_B, T]$ plane.

At the final point of the nonequilibrium expansion quarks will coalesce into mesons, baryons and antibaryons, based on the phase space arguments used in [23]. The rate of recombination is given by

$$q + \overline{q} \to m : \dot{n}_m = C_m \frac{g_m}{g_q g_{\bar{q}}} n_q \overline{n}_q, \quad (29)$$

$$q + q + q \to b : \dot{n}_b = C_b \frac{g_b}{g_q g_q g_q} n_q n_q n_q, \quad (30)$$

$$\overline{q} + \overline{q} + \overline{q} \to \overline{b} : \dot{\overline{n}}_b = C_b \frac{g_b}{g_q g_q g_q} \overline{n}_q \overline{n}_q \overline{n}_q. \quad (31)$$

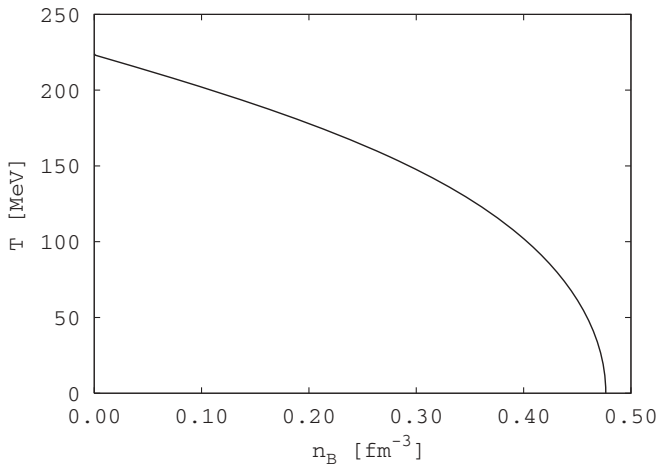

FIG. 3. The initial conditions for nonequilibrium expansion are determined by vanishing quark condensate; see Eqs. (7) and (8). This corresponds to temperature and density conditions where constituent quark mass equals current quark mass $M_f = m_f$ according to Eq. (10).

Here, q ($\overline{q}$) denotes quarks (antiquarks), m denotes mesons, b ($\overline{b}$) denotes baryons (antibaryons), g_m and g_b are mesonic and baryonic degeneracy factors, and the coefficients C_m and C_b should be determined by including phase space factors and an additional normalization constant to satisfy the following relations. Notice that the same statistical phase-space factors appear in coalescence rates and in the statistical thermal model if the overlap integrals of the coalescing constituents are similar. Eventually other channels via di-quark formation can also be taken into account, and the time-integrated solution will provide the final hadron abundances.

On the other hand the baryon charge is the excess number of baryons over antibaryons, and this leads to the normalization requirements for the final hadrons:

$$n_B = n_b - \overline{n}_b. \tag{32}$$

Thus, a fraction "a" of the antiquarks may form antibaryons:

$$\overline{n}_b = a\,\frac{\overline{n}_q}{3}, \qquad n_b = \frac{n_q - \overline{n}_q}{3} + a\,\frac{\overline{n}_q}{3}, \tag{33}$$

and the rest of the quarks form mesons:

$$n_m = (1-a)\,\overline{n}_q. \tag{34}$$

The only coefficient, a, should arise from the coalescence factors above. Initially from Eqs. (30)–(31) the ratio of formed baryons and antibaryons is $n_b/\overline{n}_b = Q^3$, where $Q \equiv n_q/\overline{n}_q$. Assuming that the initial recombination is dominant the conservation laws then yield

$$a \approx \frac{Q-1}{Q^3-1}. \tag{35}$$

The full integration of the rate equations may lead to a change of a, which would modify the ratio of antibaryons to mesons to a smaller extent. In Ref. [23] the same coalescence model explained the constituent quark number scaling of the flow parameter, v_2, from a weak elliptic asymmetry of the coalescing quark distributions.

In this way at any stage of expansion, from an initial volume V_0 to a point at time t with a given volume $V(t)$, we can get all the meson and baryon densities and masses, as well as the total energy from energy conservation (neglecting the mechanical work done by the negligible pressure).

From the baryon and meson densities n_B and n_m and the hadronic energy density, E_H, we can calculate the baryon and meson chemical potentials (the meson density may exceed the thermal equilibrium value), μ_B and μ_m, and the respective temperatures $T_b(t)$ and $T_m(t)$. Notice that with the broken chemical equilibrium the equality of chemical potentials is broken. In this rapid hadronization process the thermal, pressure, and flow equilibrium will also break down. Thus the details of how this happens should be described in terms of extensive variables as we will see in the next section.

B. Choice of initial conditions

Let us consider now the initial conditions for all these parameters. The applicability of Eq. (10) is restricted by the condition that the constituent quark mass has to be positive. Accordingly, we will take the initial conditions such that in the initial state the in-medium chiral condensate $\langle \overline{q}q \rangle_{n_B,T}$ vanishes and quarks have a current quark mass. This condition implies that the density and temperature-dependent terms in Eq. (10) are equal to 1. The corresponding curve in the temperature-density plane is shown in Fig. 3. We used for the current quark mass $m_f = 7\,\mathrm{MeV}$, ignoring the difference between u- and d-quarks.

In this model it is assumed that the chemical equilibrium between the quarks and antiquarks breaks precisely on this curve, and the quark and antiquark numbers are conserved separately during further expansion. At the earlier stage, the quark and antiquark numbers, N_q and $\overline{N}_q$, are computed from the temperature T and baryon number density n_B using Eqs. (26), (24), and (25) with chemical potentials $\mu_q = \mu_B/3$ and $\overline{\mu}_q = -\mu_B/3$. But after crossing the line on Fig. 3 the numbers of quarks and antiquarks, N_q and $\overline{N}_q$, are assumed to stay constant. During further expansion μ_q and $\overline{\mu}_q$ change separately and can be obtained numerically from the quark and antiquark densities, n_q and $\overline{n}_q$, by means of Eqs. (24) and (25). Because this is a nonequilibrium model, all numerical calculations are carried out on the $[n_B, T]$ plane, using the densities n_B, n_q, $\overline{n}_q$ and the temperature T (and not on the $[\mu_B, T]$ plane).

C. Expansion of the quark gas

The expansion of the gas of quarks and antiquarks is considered to be adiabatic (i.e., at constant entropy). The initial total entropy density of the gas, s_0, can be calculated from the initial temperature, T_0, and initial baryon charge density, n_B^0, assuming chemical equilibrium between the quarks and antiquarks (i.e., $\mu_q = -\overline{\mu}_q = \mu_B/3$), and using Eq. (26) to get the chemical potential and substituting it into Eqs. (17), (18), and (19).

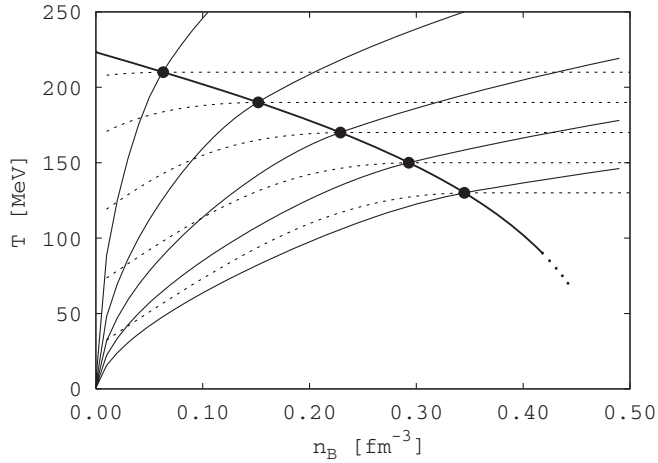

FIG. 4. Expansion of the gas of quarks and antiquarks. The thick solid line is calculated assuming the quark masses to be equal to the current quark mass, that means it is identical to the curve in Fig. 3. Beyond that curve we take $M_f = m_f$. The dots on the thick solid line indicate the initial temperature and initial baryonic density for each curve of adiabatic and iso-ergic expansion. The thin solid lines represent the trajectories of the adiabatic expansion of the gas of quarks and antiquarks. The trajectories of the iso-ergic dissipative expansion (dotted lines) are plotted for comparison.

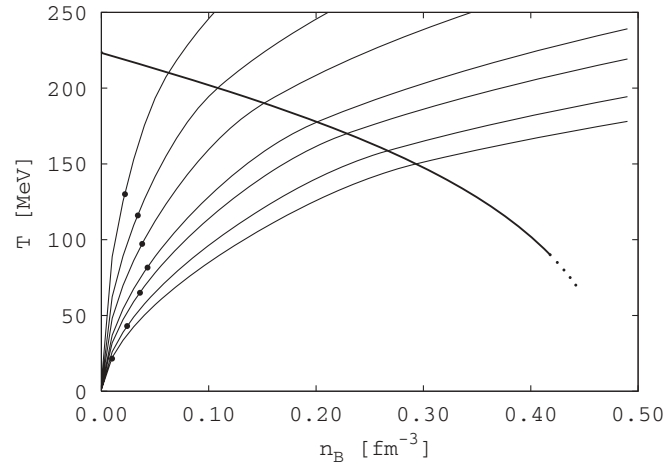

FIG. 5. A series of curves of adiabatic expansion (thin solid lines) of the gas of quarks and antiquarks. The dots on the adiabatic expansion curves indicate where the rapid freeze-out and hadronization happens. These points are determined based on the condition that the energy of the system, including the background field, divided by the estimated number of hadrons reaches 1.2 GeV hadron. The thick solid line is the same as in Fig. 3.

After the initial moment, the quark and antiquark densities decrease inversely proportionally to the volume V of the system: $n_q = V_0/V\, n_q^0, \overline{n}_q = V_0/V\, \overline{n}_q^0, n_B = V_0/V\, n_B^0$, where V_0 is the initial volume. Then the total entropy of the system can be expressed simply as a function of volume, temperature, and numerically obtained chemical potentials (or temperature and baryon density) using Eqs. (17), (18), and (19).

Using the condition that the total entropy is constant [i.e., the entropy density also decreases as $s(T, V) = s_q(T, V) + \overline{s}_q(T, V) = V_0/V\, s_0$], the expansion trajectories on the $[n_B, T]$ plane can be calculated numerically. These trajectories are plotted in Fig. 4. The trajectories corresponding to constant energy expansion (iso-ergic) were calculated, in a similar way, using Eqs. (14) and (15). This case corresponds to a dissipative expansion. It is apparent from Fig. 4 that the adiabatic expansion where $s = s_0\, n_B/n_B^0$ leads to the fastest temperature decrease than the iso-ergic one where $e = e_0\, n_B/n_B^0$.

D. Recombination into hadrons

Because of confining forces, the quarks will finally recombine into hadrons. We assume that this happens rapidly at the point of recombination when the average energy per hadron (including the background field) decreases to $E_H/N_H = 1.2$ GeV, a value that is still above the values of (1.0–1.1) GeV obtained by Cleymans *et al.* [3]. This corresponds nearly to the energy per hadron of the empirically observed freeze-out. The end points of the expansion curves where the recombination happens are shown in Fig. 5.

The quarks are assumed to recombine into three types of particles: baryons, antibaryons, and mesons, which contain three quarks, three antiquarks, or a quark and an antiquark, respectively. All hadrons are assumed to have a mass that is the sum of the masses of their constituent quarks at the freeze-out, that is,

$$M_b = \overline{M}_b = 3\, M_f\left(n_B^{\mathrm{FO}}, T^{\mathrm{FO}}\right), \tag{36}$$

$$M_m = 2\, M_f\left(n_B^{\mathrm{FO}}, T^{\mathrm{FO}}\right). \tag{37}$$

Further differences between the various hadron species are disregarded. Most of the antiquarks will pair with quarks to form mesons, but a small fraction, a, will form antibaryons. This ratio, a, can be estimated based on the recombination rates given in Ref. [23]. Thus the baryon, antibaryon, and meson densities n_b, $\overline{n}_b$, and n_m are calculated from the quark and antiquark densities (n_q and $\overline{n}_q$) using Eqs. (33), (34), and (35).

We assume that at the point of recombination the flow freezes out, too, and both the thermal and chemical equilibria cease. The hadrons are assumed to have Jüttner distribution after the freeze-out, but the temperature parameter in this distribution will be different for baryons and mesons. The parameters of the distribution after recombination are calculated from the condition of energy conservation: The thermal energy of each hadron type will be equal to the energy of their constituent quarks, $E_m^{\mathrm{th}} = E_b^{\mathrm{th}}$. Because of the different masses of baryons and mesons, their temperature parameters will be different. The temperature ratio T_b/T_m will correspond to the mass ratio $M_b/M_m = 3/2$. The distributions of baryons and mesons for a calculation done with initial state $n_B^0 = 0.21\ \mathrm{fm}^{-3}$ and $T_0 = 176$ MeV is shown in Figs. 6 and 7. Here the final baryon and meson temperatures are $T_b = 228$ MeV and $T_m = 152$ MeV and $T_b/T_m = 3/2$, whereas the final constituent quark mass is 308 MeV. The scaled p_{t} and E_{t} distributions become identical under this condition, however, this is not enough to reproduce the NCQ scaling of $v_2(p_{\mathrm{t}})$ indicating that the recombination influences the flow velocities of the final

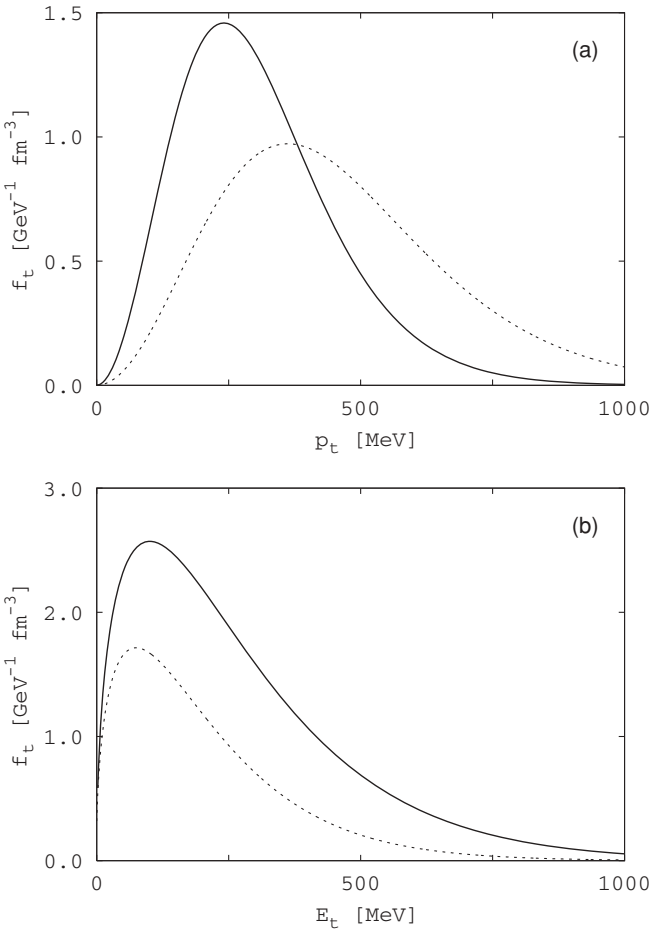

FIG. 6. Baryon (dotted) and meson (solid) distributions as functions of transverse momentum p_t (a) and transverse energy E_t (b), for the case of an adiabatic expansion. The initial state for this calculation was $n_B^0 = 0.21\,\mathrm{fm}^{-3}$ and $T_0 = 176\,\mathrm{MeV}$.

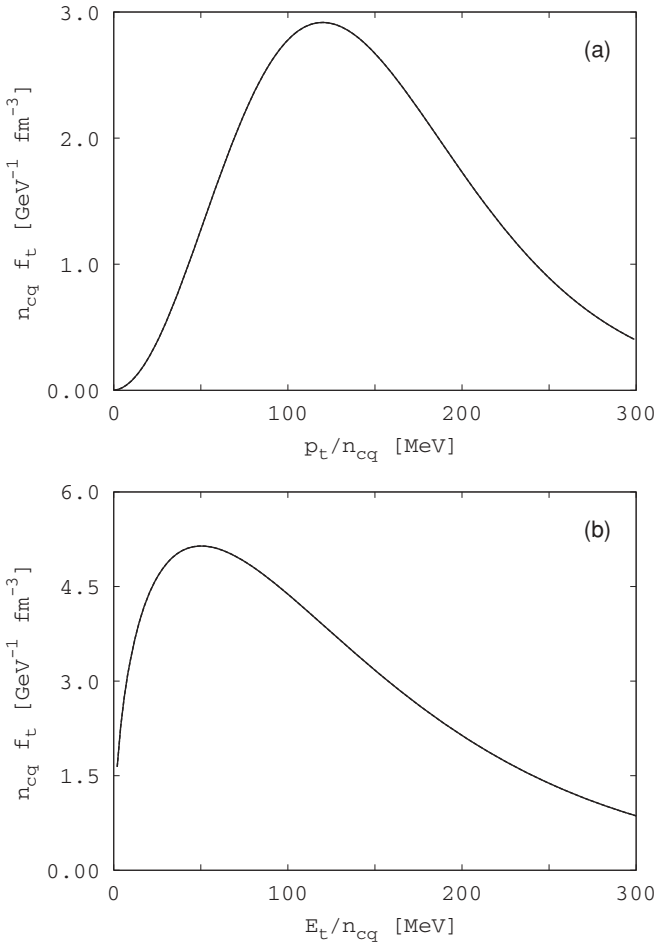

FIG. 7. These diagrams show the same distribution functions for baryon (dotted) and meson (solid) as calculated in Fig. 6, but rescaled according to constituent quark number n_{cq} ($n_{cq} = 3$ for baryons, $n_{cq} = 2$ for mesons). (a) Shows the scaled distribution $n_{cq}\, f_t$ as a function of rescaled transverse momentum $n_{cq}\, p_t$. (b) Shows the rescaled distribution $n_{cq}\, f_t$ as a function of rescaled transverse energy $n_{cq}\, E_t$. These rescaled distributions almost coincide for baryons and mesons; they are on top of each other so no difference can be seen here in the diagrams. The initial state for this calculation was $n_B^0 = 0.21\,\mathrm{fm}^{-3}$ and $T_0 = 176\,\mathrm{MeV}$.

hadrons. This concept was already pointed out in Ref. [23] based on the properties of the collision integral. It is important to point out that the transport theoretical treatment and the collision integral are applicable also at situations when the local equilibrium has ceased to exist.

V. ELLIPTIC FLOW

The elliptic flow parameter, v_2, can be calculated from the final, post freeze-out distribution by the Cooper-Frye formula. Assuming an isochronous FO hypersurface, we obtain simple expressions for final measurables [24].

A. Formula for the elliptic flow

In this section we mainly follow the arguments of Refs. [24,25]. The kinematic average of a quantity $A(\boldsymbol{x}, \boldsymbol{p})$ is given by

$$\langle A \rangle = \frac{\int d^3x \int d^3p\; f(\boldsymbol{x}, \boldsymbol{p})\, A(\boldsymbol{x}, \boldsymbol{p})}{\int d^3x \int d^3p;\, f(\boldsymbol{x}, \boldsymbol{p})}, \tag{38}$$

where $f(\boldsymbol{x}, \boldsymbol{p})$ is the one-particle distribution function. Especially, we are interested in the elliptic flow v_2, that is, the following kinematic average:

$$v_2 = \left\langle \frac{p_x^2 - p_y^2}{p_t^2} \right\rangle. \tag{39}$$

According to Eqs. (38) and (39), we obtain

$$v_2 = \frac{\int d^3x \int d^3p\; f(\boldsymbol{x}, \boldsymbol{p})\, \frac{p_x^2 - p_y^2}{p_t^2}}{\int d^3x \int d^3p\; f(\boldsymbol{x}, \boldsymbol{p})}. \tag{40}$$

Now we subdivide the system into N fireballs or cells, each of which has a given volume V_i and contains a given number of particles N_i, which are distributed by a given distribution function $f_i(\boldsymbol{x}, \boldsymbol{p})$ inside cell i. Because in a given cell the

elliptic flow parameter v_2 does not depend on coordinate $\boldsymbol{x}$, we can take the integral over d^3x and obtain

$$v_2 = \frac{\sum_{i=1}^{N} V_i \int_0^{2\pi} d\phi \int_0^{\infty} dp_{\parallel} \int_0^{\infty} dp_{\mathrm{t}}\, p_{\mathrm{t}}\, f^i(\boldsymbol{p})\, \cos 2\phi}{\sum_{i=1}^{N} V_i \int_0^{2\pi} d\phi \int_0^{\infty} dp_{\parallel} \int_0^{\infty} dp_{\mathrm{t}}\, p_{\mathrm{t}}\, f^i(\boldsymbol{p})}, \tag{41}$$

where we have used the relation $\cos 2\,\phi = \cos^2\phi - \sin^2\phi = \frac{p_x^2}{p_{\mathrm{t}}^2} - \frac{p_y^2}{p_{\mathrm{t}}^2}$ with $p_{\mathrm{t}} = \sqrt{p_x^2 + p_y^2}$ being the transverse momentum. In our study we consider the midrapidity particles, ($p_z = 0$ or the rapidity $y = 0$) [i.e., $\boldsymbol{p} = (p_x, p_y)$] and there is no integration for the longitudinal momentum or rapidity. Furthermore, we are interested in the momentum dependence of elliptic flow parameter v_2. Thus we obtain from (41) the following expression:

$$v_2\,(p_{\mathrm{t}}, y = 0) = \frac{\sum_{i=1}^{N} V_i \int_0^{2\pi} d\phi\; f^i(p_x, p_y)\, \cos 2\phi}{\sum_{i=1}^{N} V_i \int_0^{2\pi} d\phi\; f^i(p_x, p_y)}, \tag{42}$$

where the sum runs over all individual cells $i = 1, ..., N$, and we have used the fact that for midrapidity particles $\boldsymbol{p}^2 = p_x^2 + p_y^2 = \boldsymbol{p}_{\mathrm{t}}^2$. Let us study the elliptic flow of a single type of particle. We assume a Jüttner distribution in each individual cell of the bag; see Eq. (12), and obtain

$$\begin{aligned} f_{\mathrm{J}}^i &= \frac{1}{(2\,\pi\,\hbar)^3} \exp\left(\frac{\mu^i - \gamma_i\, p_0^i + \gamma^i\, v_x^i\, p_x + \gamma^i\, v_y^i\, p_y}{T_i}\right) \\ &= \frac{1}{(2\,\pi\,\hbar)^3} \exp\left(\frac{\mu^i - \gamma_i\, p_0^i + \gamma^i\, v^i\, p_v}{T_i}\right), \end{aligned} \tag{43}$$

where p_v is the component of the momentum parallel to the cell velocity $\mathbf{v}^i$, and μ^i is the chemical potential of the given particle type in the cell i; here we have also used $u_i^{\mu} = \gamma^i(1, v_x^i, v_y^i, 0)\,, \quad u_{\mu}^i = \gamma^i(1, -v_x^i, -v_y^i, 0)$ and $p^{\mu} = (p_0, p_x, p_y, 0)\,, \quad p_{\mu} = (p_0, -p_x, -p_y, 0)$. Because the elliptic flow parameter is calculated after chemical freeze-out has happened, each particle type has their own chemical potential,

$$\frac{1}{(2\pi\hbar)^3} \exp\left(\frac{\mu^i}{T}\right) = \frac{n_i}{4\pi\, M_i^2\, T_i\, K_2(M_i/T_i)}, \tag{44}$$

where n_i is the density and M_i is the mass of the given particle type. For particles at CM rapidity the zeroth component of four-momentum equals the transverse mass (i.e., it is just the energy of one particle),

$$p_0^i = \sqrt{M_i^2 + p_{\mathrm{t}}^2} = M_{\mathrm{t}}^i. \tag{45}$$

Then, according to Eqs. (42) and (43), we obtain the following expression for the elliptic flow:

$$v_2 = \frac{\sum_{i=1}^{N} V_i \int_0^{2\pi} d\phi\, \cos 2\phi\, f_{\mathrm{J}}^i(p_x, p_y)}{\sum_{i=1}^{N} V_i \int_0^{2\pi} d\phi\, f_{\mathrm{J}}^i(p_x, p_y)}, \tag{46}$$

where the sum runs over all cells of the bag. Now let us insert Eq. (43) into expression (46). Then, by means of Eq. (44) we obtain the following expression for the v_2 parameter:

$$v_2 = \frac{\sum_{i=1}^{N} \tilde{N}_i\, e^{-\gamma^i M_{\mathrm{t}}^i/T_i} \int_0^{2\pi} d\phi\, \cos 2\phi\, e^{\gamma^i\, v_i\, p_v/T_i}}{\sum_{i=1}^{N} \tilde{N}_i\, e^{-\gamma^i\, M_{\mathrm{t}}^i/T_i} \int_0^{2\pi} d\phi\, e^{\gamma^i\, v_i\, p_v/T_i}}, \tag{47}$$

where $\tilde{N}_i$ denotes

$$\tilde{N}_i = V_i\, \frac{n_i}{T_i\, K_2(M_i/T_i)}. \tag{48}$$

If the direction of the velocity of cell i relative to axis x is denoted by ϕ_0^i, then p_v can be written as $p_v = p_{\mathrm{t}} \cos(\phi - \phi_0)$, and the following expression is obtained:

$$v_2(p_{\mathrm{t}}) = \frac{\sum_{i=1}^{N} \tilde{N}_i\, e^{-\gamma^i M_{\mathrm{t}}^i/T_i}\, \cos 2\phi_0^i\, I_2(\gamma^i\, v_i\, p_{\mathrm{t}}/T_i)}{\sum_{i=1}^{N} \tilde{N}_i\, e^{-\gamma^i M_{\mathrm{t}}^i/T_i}\, I_0(\gamma^i\, v_i\, p_{\mathrm{t}}/T_i)}. \tag{49}$$

I_0 and I_2 denote the zeroth- and second-order modified Bessel functions of the first kind [26].

Notice that if the source temperatures are all equal or if the freeze-out temperature of all fluid cells is the same, than one observes a linear increase of v_2 as a function of p_{t} or $p_{\mathrm{t}}/n_{\mathrm{cq}}$. This is frequently quoted as a linear hydrodynamical increase, observed already in the first model calculations (e.g., [24]). Such linear increase leads trivially to a constituent quark number scaling. It is easy to see that this feature is just a consequence of the equal temperature assumption. If, for example, we assume a large, hotter, static central source, the high p_{t} behavior of v_2 will be dominated by this hot source and thus v_2 will decrease at high p_{t} as pointed out in Ref. [25].

If we assume that the temperatures of all cells are the same, $T_i = T$, then the temperature- and mass-dependent parts of $\tilde{N}_i$ [see Eq. (48)] cancel from the numerator and denominator of Eq. (49), and we get (note at FO the constituent quark mass does not depend on density and temperature anymore)

$$v_2(p_{\mathrm{t}}) = \frac{\sum_{i=1}^{N} N_i e^{-\gamma^i M_{\mathrm{t}}^i/T}\, \cos 2\phi_0^i\, I_2(\gamma^i\, v_i\, p_{\mathrm{t}}/T)}{\sum_{i=1}^{N} N_i e^{-\gamma^i M_{\mathrm{t}}^i/T}\, I_0(\gamma^i\, v_i\, p_{\mathrm{t}}/T)}. \tag{50}$$

In the special case of four cells moving into the four directions ($\pm x, \pm y$), Eq. (50) reduces to the expression given in Ref. [24].

The simplest configuration that can approximate elliptic flow is dividing the system into two cells that move in opposite directions with the same velocity v. For this "two-cell" model case the v_2 parameter is expressed as

$$v_2(p_{\mathrm{t}}) = \frac{I_2(\gamma\, v p_{\mathrm{t}}/T)}{I_0(\gamma\; v\; p_{\mathrm{t}}/T)}. \tag{51}$$

A slightly more complicated possibility is having one larger nonmoving central cell, and two smaller side cells moving in opposite directions, as shown in Fig. 8. In this "three-cell" model case $v_2(p_{\mathrm{t}})$ can be expressed as

$$v_2(p_{\mathrm{t}}) = \frac{2N_s\, e^{-\gamma M_{\mathrm{t}}/T} I_2(\gamma\; v\; p_{\mathrm{t}}/T)}{2N_s\, e^{-\gamma M_{\mathrm{t}}/T} I_0(\gamma\; v\; p_{\mathrm{t}}/T) + N_c\, e^{-M_{\mathrm{t}}/T}}. \tag{52}$$

Here N_c denotes the particle number of the central cell, whereas N_s denotes the particle number of the identical side cells. This configuration corresponds to a flow with less pronounced asymmetry. The large central cell has a

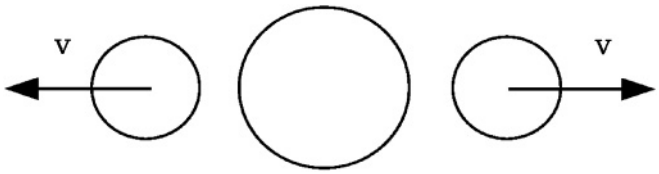

FIG. 8. Scheme of three-cell model. The asymmetric flow is approximated by dividing the system into either two cells that move in opposite direction with velocity v, or two smaller moving side cells and a stationary central cell. The schematic of the latter configuration is shown here.

spherical momentum distribution, whereas the smaller side cells introduce a slight asymmetry to this.

B. Calculation of the elliptic flow

1. Two-cell model

As a first approximation, the v_2 parameter was calculated using a simple model of elliptic flow where the system is divided into two droplets moving in opposite directions with the same velocity. For this model, v_2 is given by Eq. (51).

The baryons and mesons were given different flow energies, such that the ratio of flow energy per quark is $(FE_b/n_{\rm cq})/(FE_m/n_{\rm cq}) = 3/2$. This leads to different flow velocities for baryons and mesons, and reproduces the constituent quark number scaling of the elliptic flow parameter. In this model the scaling according to the transverse momentum p_t and transverse energy $E_{\rm t}$ are tied to each other (i.e., the scaling is either present or not for both these variables). By this point of the evolution of our system, all energy in the background field is exhausted and the internal, excitation, and random kinetic energies of the hadrons reach the FO value (1.0–1.1) GeV.

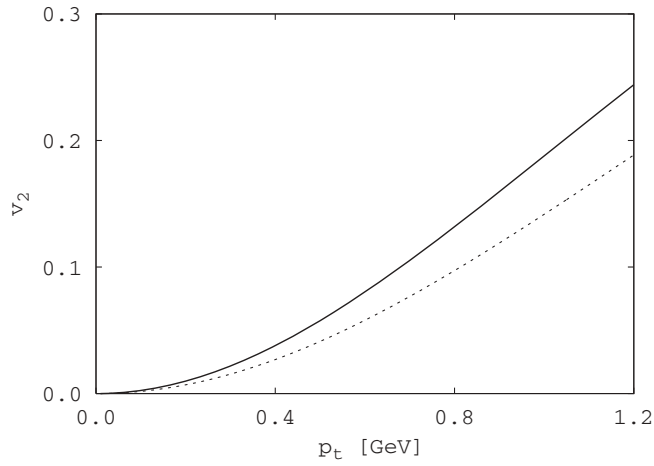

FIG. 9. The v_2 parameter as a function of $p_{\rm t}$, calculated from the two-cell model, Eq. (51). The initial state used is the same as in Figs. 6 and 7. The dotted curve represents the baryons, whereas the solid curve represents the mesons. The cell velocities for baryons and mesons are $v_b = 0.26$ and $v_m = 0.21$, corresponding to a flow-energy ratio of 3:2 of the constituent quarks of the two different particle types (calculated relativistically).

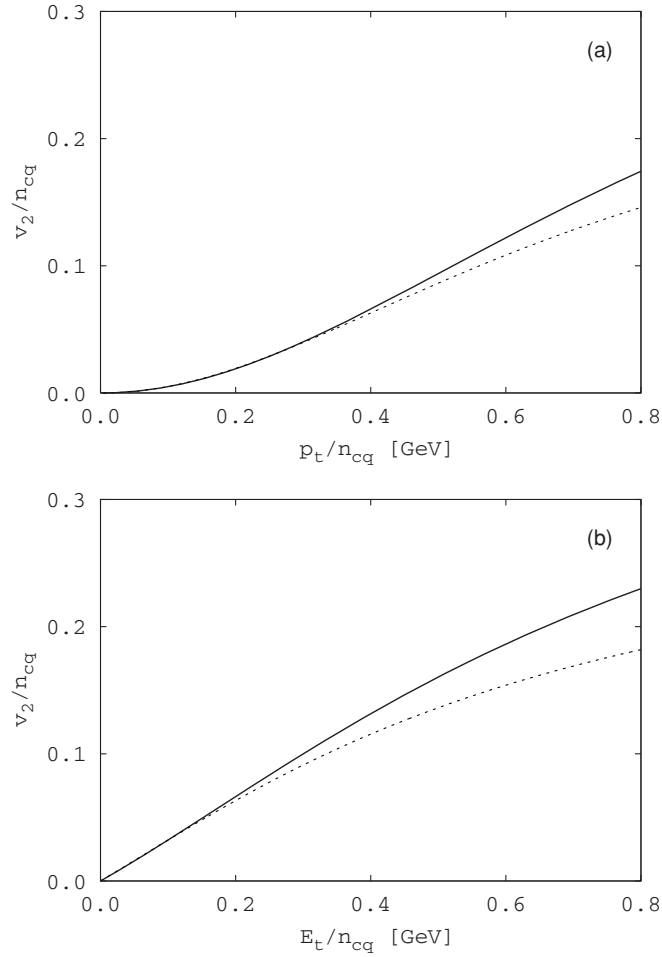

FIG. 10. The rescaled elliptic flow parameter, $v_2/n_{\rm cq}$, as a function of $p_{\rm t}/n_{\rm cq}$ (a) and $E_{\rm t}/n_{\rm cq}$ (b), calculated from the two-cell model. The dotted curves represent the baryons while the solid curves represent the mesons. The curves coincide for low $p_{\rm t}$ value (i.e., the constituent quark number scaling is reproduced for the low $p_{\rm t}$ region).

The $v_2(p_{\rm t})$ curve obtained with the initial state parameters discussed in the previous section is shown in Fig. 9. The elliptic flow parameter, rescaled according to constituent quark number is shown in Fig. 10. In this figure, the baryon and meson curves coincide for low $p_{\rm t}$ (i.e., constituent quark number scaling of v_2 is reproduced for small values of the transverse momentum, but not for $p_{\rm t} > 400$ MeV). These results of QNS can be further improved by considering a three-cell model, as we will see in the next subsection.

2. Three-cell model

The asymmetry in the two-cell model described in the previous subsection is very strong. In Ref. [23] it is shown that the constituent quark number scaling is more precise if the v_2 coefficient is small, and the higher harmonic coefficients v_k ($k > 2$) are negligible. Therefore, a three-cell model with one large stationary central cell and two moving side cells was also studied. The schematic scheme of this arrangement of cells is shown on Fig. 8. The elliptic flow parameter of the three-cell

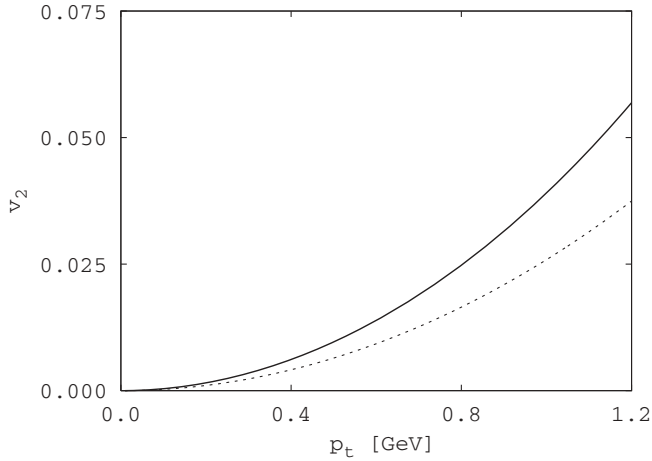

FIG. 11. The v_2 parameter as a function of p_t, calculated from the three-cell model, Eq. (52). The initial state used is the same as in Figs. 6 and 7. The dotted curve represents the baryons, whereas the solid curve represents the mesons. The cell velocities for baryons and mesons are $v_b = 0.26$ and $v_m = 0.21$, corresponding to a flow-energy ratio of 3:2 of the constituent quarks of the two different particle types (calculated relativistically). A particle ratio $N_c/N_s = 10$ was assumed.

model is given by Eq. (52) and the result is shown in Fig. 11. The side cells were assumed to have the same velocities as in the case of the two-cell model, and the temperature of all cells was the same. The particle number ratio of the central cell to the side cells was set to $N_c/N_s = 10$. It should be noticed, that the elliptic flow parameter, shown in Fig. 11, is not insensitive on such choice (e.g., a ratio of $N_c/N_s = 5$ would enlarge the value of v_2).

The elliptic flow parameter, rescaled according to constituent quark number is shown in Fig. 12. We have found that QNS is insensitive on the chosen particle number ratio $N_c/N_s = 10$ (e.g., a ratio $N_c/N_s = 5$ yields very similar results as shown in Fig. 12). According to the results in Fig. 12, the three-cell model is able to reproduce the constituent quark number scaling of v_2 for a wider range of p_t values compared to the two-cell model. It must be noted that this is not only a result of the reduction of the momentum distribution asymmetry compared to the two-cell model. However, the choice of flow velocities for baryons and mesons is still relevant.

VI. SUMMARY

A model of rapid hadronization was considered in which the effective constituent quark mass depends on density and temperature. In this model the evolution starts from an ideal QGP in chemical, thermal, and mechanical equilibrium. Then, one after the other the chemical, thermal, and mechanical equilibrium break down rapidly, while the quarks build up constituent quark mass, and the background gluon field (bag constant) breaks up and vanishes. This model can be considered as a simple representation of the breaking chiral symmetry and deconfinement in a dynamical transition crossing the Quarkyonic phase [2].

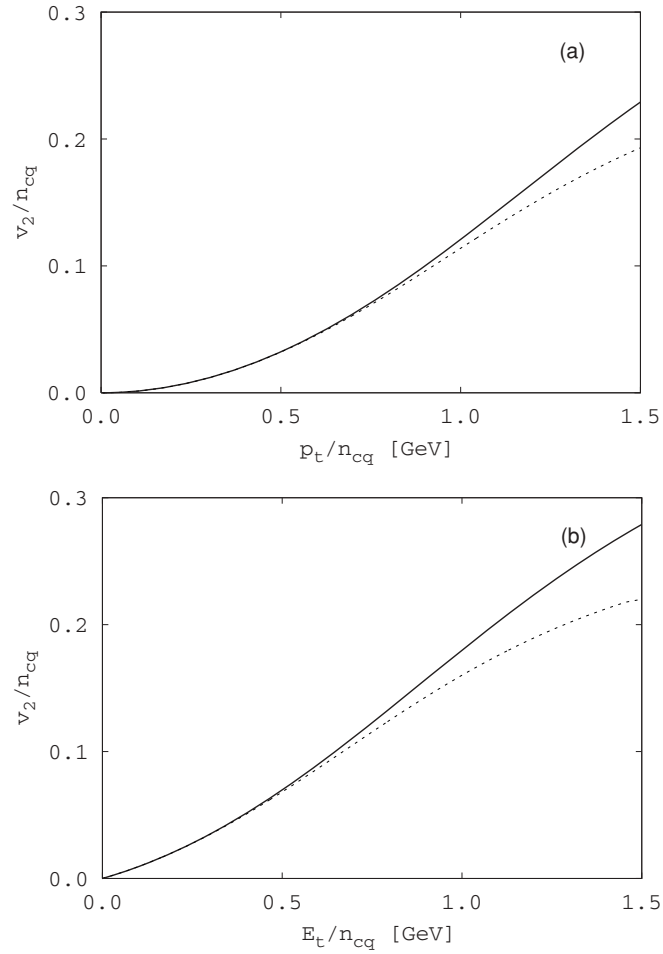

FIG. 12. The rescaled elliptic flow parameter, v_2/n_{cq}, as a function of p_t/n_{cq} (a) and E_t/n_{cq} (b), calculated from the three-cell model. The dotted curves represent the baryons whereas the solid curves represent the mesons. The curves overlap nearly completely, and the constituent quark number scaling is reproduced for a much wider range of p_t than in the case of the two-cell model. The velocities of the side sources are the same as in Fig. 9. A particle ratio $N_c/N_s = 10$ was assumed.

The elliptic flow parameter v_2 was calculated for the final hadron distributions obtained from the model, and the constituent quark number scaling was partially reproduced. We assume the following stages of hadronization: (1) The chemical equilibrium between the quarks and antiquarks breaks and the chiral symmetry breaks at the same time. (2) The quark and antiquark numbers are assumed to be conserved during further expansion (i.e., quark, antiquark pair creations and annihilations are ceased). (3) As the quark gas expands and cools, the quarks gain mass according to Eq. (10), and the field associated with the bag constant B decreases. (4) The thermal freeze-out and recombination into hadrons are completed when the mean energy per hadron reaches the FO value of $E_H/N_H = (1.0–1.1)$ GeV. The created hadrons are not in local thermal and flow equilibrium with each other. We considered only three types of hadrons: baryons, antibaryons, and mesons, ignoring the differences between

different hadron species, and the momentum distribution of hadrons was calculated.

Using the obtained momentum distributions, the elliptic flow parameter v_2 was computed from a simple multisource model of the elliptic flow. Two cases were considered. In the first case, the flow asymmetry is approximated by two fireballs moving in opposite directions. Although this leads to a very strong asymmetry in the momentum distribution, it leads to a $v_2(p_t)$ curve that scales with the constituent quark number for small p_t values only. In the second case, we added a large central fireball to reduce the asymmetry and approximate pure elliptic flow better [i.e., reduce the higher v_k $(k > 2)$ harmonic coefficients]. This three-source model was able to reproduce the constituent quark number scaling for a wide range of p_t values.

The present model is highly simplified and attempts to provide an insight to the rapid hadronization and freeze-out process in view of the quark number scaling. We considered the features arising from the breaking down of equilibrium in this process in terms of thermo and fluid dynamical parameters that are applicable to partial components of the matter. We intend to implement these concepts in more complex models (like hybrid models) and to search for more fundamental reasons for the observed freeze-out features in terms of the partial extensives.

Despite the simplicity of the model, it is capable of reproducing the constituent quark number scaling of the v_2 elliptic flow parameter. The presence of constituent quark number scaling in experimental data suggests that the elliptic flow develops in the quark-gluon plasma phase, before the quarks recombine into hadrons. Therefore understanding the origin the elliptic flow can provide insight into the quark phase of matter.

ACKNOWLEDGMENTS

Enlightening discussions with Professor Daniel D. Strottman are gratefully acknowledged. The authors also thank Dr. Kalliopi Kanaki, Yun Cheng, Dr. Csaba Anderlik, and Dr. Etele Molnar for useful hints and advice. Sven Zschocke is grateful for the sincere hospitality of the Physics Department of University of Bergen, and Magne Håvåg is acknowledged for kind computer assistance. This work was supported by the Alexander von Humboldt Foundation, by the Meltzer Fund of the University of Bergen, and by the Computational Subatomic Physics Project at Uni-Research of the Research Council of Norway. Igor N. Mishustin acknowledges partial support from DFG Grant No. 436RUS 113/957/0-1 (Germany) and Grants No. NS-7235.2010.2 and No. RFBR09-02-91331 (Russia).

[1] S. S. Adler *et al.* (PHENIX Collaboration), Phys. Rev. Lett. **91**, 182301 (2003); J. Adams *et al.* (STAR Collaboration), Phys. Rev. Lett. **92**, 052302 (2004).
[2] L. McLerran and R. D. Pisarski, Nucl. Phys. A **796**, 83 (2007).
[3] J. Cleymans, D. Elliott, A. Keranen, and E. Suhonen, Phys. Rev. C **57**, 3319 (1998); J. Cleymans, H. Oeschler, and K. Redlich, *ibid.* **59**, 1663 (1999); A. Andronik, P. Braun-Munzinger, and J. Stachel, Nucl. Phys. A **772**, 167 (2006); J. Cleymans, H. Oeschler, K. Redlich, and S. Wheaton, Acta Phys. Pol. B, Proc. Suppl. **3**, 533 (2010).
[4] S. P. Klevansky, Rev. Mod. Phys. **64**, 649 (1992).
[5] U. Vogel and W. Weise, Prog. Part. Nucl. Phys. **27**, 195 (1991).
[6] I. N. Mishustin, L. M. Satarov, H. Stöcker, and W. Greiner, Phys. Atom. Nucl. **64**, 802 (2001).
[7] H. Li and C. M. Shakin, Phys. Rev. D **66**, 074016 (2002).
[8] T. D. Cohen, R. J. Furnstahl, and D. K. Griegel, Phys. Rev. C **45**, 1881 (1992).
[9] A. I. Bochkarev and M. E. Shaposhnikov, Phys. Lett. B **145**, 276 (1984); A. I. Bochkarev and M. E. Shaposhnikov, Nucl. Phys. B **268**, 220 (1986).
[10] T. D. Cohen, R. J. Furnstahl, D. K. Griegel, and X. Jin, Prog. Part. Nucl. Phys. **35**, 221 (1995).
[11] T. Hatsuda, Y. Koike, and S. H. Lee, Nucl. Phys. B **394**, 221 (1993).
[12] S. Zschocke, O. P. Pavlenko, and B. Kämpfer, Eur. Phys. J. A **15**, 529 (2002).
[13] S. Zschocke and L. P. Csernai, Eur. Phys. J. A **39**, 349 (2009).
[14] S. Zschocke, B. Kämpfer, O. P. Pavlenko, and Gy. Wolf, arXiv:nucl-th/0202066.
[15] E. G. Drukarev and E. M. Levin, Prog. Part. Nucl. Phys. **27**, 77 (1991).
[16] P. Gerber and H. Leutwyler, Nucl. Phys. B **321**, 387 (1989).
[17] F. Jüttner, Ann. Phys. Chem. **34**, 856 (1911).
[18] Sz. Horvat, V. K. Magas, D. D. Strottman, and L. P. Csernai, Phys. Lett. B **692**, 277 (2010).
[19] L. P. Csernai and J. I. Kapusta, Phys. Rev. Lett. **69**, 737 (1992); Phys. Rev. D **46**, 1379 (1992).
[20] T. Csörgő and L. P. Csernai, Phys. Lett. B **333**, 494 (1994).
[21] L. P. Csernai and I. N. Mishustin, Phys. Rev. Lett. **74**, 5005 (1995).
[22] K. Rajagopal and F. Wilczek, Nucl. Phys. B **404**, 577 (1993); I. N. Mishustin, Phys. Rev. Lett. **82**, 4779 (1999); I. N. Mishustin, Nucl. Phys. A **681**, 56 (2001); O. Scavenius, A. Dumitru, E. S. Fraga, J. T. Lenaghan, and A. D. Jackson, Phys. Rev. D **63**, 116003 (2001); J. Randrup, Phys. Rev. Lett. **92**, 122301 (2004); G. Torrieri, B. Tomasik, and I. N. Mishustin, Phys. Rev. C **77**, 034903 (2008); A. Bessa, E. S. Fraga, and B. W. Mintz, Phys. Rev. D **79**, 034012 (2009); J. Randrup, Phys. Rev. C **82**, 034902 (2010).
[23] D. Molnar, Nucl. Phys. A **774**, 257 (2006).
[24] P. Huovinen, P. F. Kolb, U. Heinz, P. V. Ruuskanen, and S. A. Voloshin, Phys. Lett. B **503**, 58 (2001).
[25] L. P. Csernai, Y. Cheng, V. K. Magas, I. N. Mishustin, and D. Strottman, Nucl. Phys. A **834**, 261c (2010).
[26] M. Abramowitz and I. A. Stegun, *Handbook of Mathematical Functions* (Dover, New York, 1970).